NANO REVIEWS

COACTION PUBLISHING

REVIEW ARTICLE

Electric-field controlled ferromagnetism in MnGe magnetic quantum dots

Faxian Xiu[1]*, Yong Wang[1,2], Jin Zou[2] and Kang L. Wang[1]*

[1]Device Research Laboratory, Department of Electrical Engineering, University of California, Los Angeles, California; [2]Materials Engineering and Centre for Microscopy and Microanalysis, University of Queensland, Brisbane, Australia

Received: 6 December 2010; Revised: 2 February 2011; Accepted: 13 February 2011; Published: 7 March 2011

Abstract

Electric-field control of ferromagnetism in magnetic semiconductors at room temperature has been actively pursued as one of the important approaches to realize practical spintronics and non-volatile logic devices. While Mn-doped III-V semiconductors were considered as potential candidates for achieving this controllability, the search for an ideal material with high Curie temperature ($T_c > 300$ K) and controllable ferromagnetism at room temperature has continued for nearly a decade. Among various dilute magnetic semiconductors (DMSs), materials derived from group IV elements such as Si and Ge are the ideal candidates for such materials due to their excellent compatibility with the conventional complementary metal-oxide-semiconductor (CMOS) technology. Here, we review recent reports on the development of high-Curie temperature $Mn_{0.05}Ge_{0.95}$ quantum dots (QDs) and successfully demonstrate electric-field control of ferromagnetism in the $Mn_{0.05}Ge_{0.95}$ quantum dots up to 300 K. Upon the application of gate-bias to a metal-oxide-semiconductor (MOS) capacitor, the ferromagnetism of the channel layer (i.e. the $Mn_{0.05}Ge_{0.95}$ quantum dots) was modulated as a function of the hole concentration. Finally, a theoretical model based upon the formation of magnetic polarons has been proposed to explain the observed field controlled ferromagnetism.

Keywords: *diluted magnetic semiconductors*; *spintronics*; *non-volatile*; *$Mn_{0.05}Ge_{0.95}$*; *quantum dots*; *electric-field controlled ferromagnetism*; *magnetic polarons*

Electric-field control of ferromagnetism has a potential to realize spin field-effect transistors (spin FETs) and non-volatile spin logic devices *via* carrier-mediated effect (1, 2). With the manipulation of carrier spins, a new generation of non-volatile (green) computing systems could be eventually developed for many low-power-dissipation applications in all fields including sensor network, health monitoring, information,

Faxian Xiu received his PhD in Electrical Engineering from the University of California, Riverside. He is now a staff research associate at the University of California, Los Angeles. He is also associated with the Functional Engineered Nano Architectonics Center (FENA) and Western Institute of Nanoelectronics (WIN) at UCLA. He is interested in dilute magnetic semiconductor nanostructures and emerging topological insulators for spintronics applications.

Yong Wang, a Research Fellow at University of Queensland, received his PhD in Condensed Matter Physics from the Institute of Physics, Chinese Academy of Sciences in 2006. He is currently a visiting scholar in Professor Kang L. Wang's group at the University of California, Los Angeles. His research interests focus on structural characterization of magnetic semiconductors, monolayer nanosheets, topological insulators, and related device fabrications and property measurements.

Jin Zou received his PhD in Materials Physics from the University of Sydney and worked there for 10 years as a researcher. He is now a professor (Chair in nanoscience) at the University of Queensland. His research interests focus on the nanocharacterization of various semiconductor and functional nanostructures; and he published over 300 journal publications in this field. In 2010, Professor Zou was awarded an Australian Future Fellowship.

Citation: Nano Reviews 2011, **2:** 5896 - DOI: 10.3402/nano.v2i0.5896

sustainable wireless system, and so on. Since Datta and Das (3) first introduced the concept of spin FETs in 1990, enormous efforts were dedicated to creating a device wherein the carrier transport is modulated by electrostatic control of carrier spins (4–12). One of major challenges, however, is to search an ideal material with room temperature controllable spin states (4–7). In recent years, emerged dilute magnetic semiconductors became one of the promising candidates since they could possibly offer high T_c in excess of 300 K (8). The demonstration of the carrier-mediated ferromagnetism involving correlated electron/hole systems leads to a para- to ferromagnetism phase transition (2, 8–10). In principle, the collective alignment of spin states in these DMSs can be manipulated by the modulation of carrier concentrations through gate-biasing in a FET structure (6, 11). For this kind of spin FETs, the 'source' and 'drain' may be completed through 'nanomagnet', which are in turn controlled by the gate and no carrier transport is needed. Clearly, one may also involve the control of source-drain conductance by gate-voltage-induced precession of injected spins (from the source). Since the early 2000s, a significant progress on electric-field controlled ferromagnetism was achieved (2, 11–13) in which the ferromagnetism of a (In, Mn)As channel layer could be effectively turned on and off *via* electric-fields in a gated FET. Such an extraordinary field modulated ferromagnetism immediately rendered the development of future spintronic devices. However, the manipulation of ferromagnetism was limited because of low T_c of the Mn-doped III-V materials (14). Therefore, a search for new DMS materials with $T_c > 300$ K and carrier-mediated ferromagnetism becomes a current global challenge (6, 15).

Importance of MnGe-based dilute magnetic semiconductors

In recent years, Mn-doped Ge DMS has attracted extensive attention because of its compatibility with today's Si microelectronics and the possibility to have higher Curie temperatures than those of group III-V materials (9, 16–19). In particular, MnGe nanostructures such as QDs may offer unique and salient physical properties arising from size and quantum confinement effects, affecting carrier transport, spin lifetimes, and interactions of spins and, thus, ferromagnetic properties (20). With this motivation we had previously investigated the magnetic properties of Mn_xGe_{1-x} nanostructures by ion implantation of Mn (10). We demonstrated the hole-mediated effect in Mn_xGe_{1-x} nanostructures and the modulation of their ferromagnetism by applying gate-biases in MOS capacitors at a low temperature of 10 K. However, the metallic precipitates such as Mn_5Ge_3 and $Mn_{11}Ge_8$ and implantation damages were found in these nanostructures, which made the system rather complex and might have partly jeopardized the hole-mediated effect. In the present research, we demonstrate our successful development of high-Curie temperature self-assembled $Mn_{0.05}Ge_{0.95}$ QDs by molecular-beam epitaxy (MBE). The structural and magnetic characterizations confirm the formation of single-crystalline DMS QDs without observable Mn_5Ge_3 or $Mn_{11}Ge_8$ precipitates. The Curie temperature of the material was measured by a superconducting quantum interference device (SQUID) magnetometer and obtained by the Arrott plots, showing T_c above 400 K. By using a similar MOS device structure as illustrated in Chen et al. (10), the effective manipulation of ferromagnetism of these QDs was clearly observed at 300 K. The fact that the $Mn_{0.05}Ge_{0.95}$ QDs possess high-Curie temperature and the room temperature electric-field-controlled ferromagnetism makes it technologically possible to fabricate practical spin devices, which can be operable at room temperature.

Kang L. Wang received his PhD from the Massachusetts Institute of Technology. He is currently an endowed Raytheon Professor of Physical Science and Electronics at the Electrical Engineering Department of the University of California, Los Angeles. He holds more than 20 patents and published over 400 papers. He received many awards including SIA University Research Award (2009), IBM Faculty Award, Guggenheim Fellow, IEEE Fellow, Semiconductor Research Corporation Inventor Awards, and the Semiconductor Research Corporation Technical Excellence Achievement Award. His research interest includes semiconductor nano devices, quantum information devices, spintronics/ferromagnetic materials and devices, and quantum structures and devices. He also serves as the Director of Marco Focus Center on Functional Engineered Nano Architectonics (FENA) and Western Institute of Nanoelectronics (WIN).

Growth and structural characterization of $Mn_{0.05}Ge_{0.95}$ quantum dots

The $Mn_{0.05}Ge_{0.95}$ QDs were grown on *p*-type Si substrates by a Perkin-Elmer solid-source MBE system. High-purity Ge (99.9999%) and Mn (99.99%) sources were evaporated by conventional high-temperature effusion cells. The self-assembled $Mn_{0.05}Ge_{0.95}$ DMS quantum dots were subsequently deposited at 450°C with a Ge growth rate of 0.2 Å/s and an adjustable Mn flux as the dopant source. The nominal thickness was designed to be 1.2 nm. A high-resolution TEM (HRTEM) image reveals that a QD has a dome shape with a base diameter of about 30 nm and a height of about 8 ~ 10 nm (Fig. 1a). The interface between the dot and the Si substrate has

Citation: Nano Reviews 2011, **2**: 5896 - DOI: 10.3402/nano.v2i0.5896

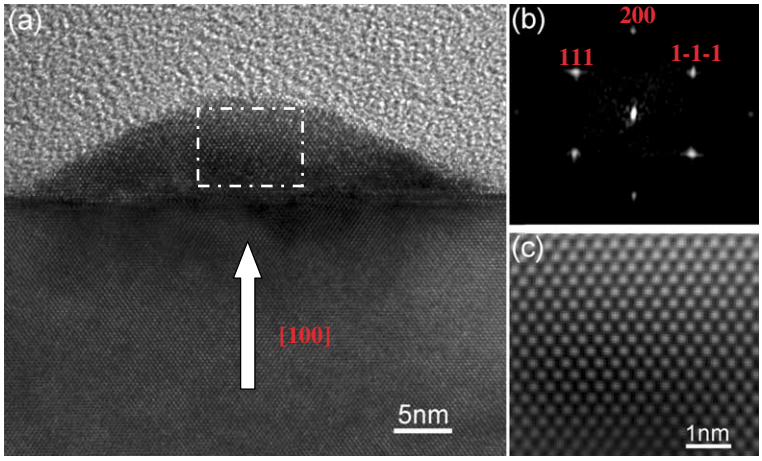

Fig. 1. (a) A cross-section TEM of $Mn_{0.05}Ge_{0.95}$ QD, (b) a fast Fourier transformation (FFT – equivalent to electron diffraction), (c) a high-resolution TEM image of the MnGe lattice through the Fourier filter, showing a perfect coherence. No amorphous layers associated with Mn oxidation were found. (Reproduced with permission from Ref. (21), copyright 2010 Nature Publishing Group.

excellent lattice coherence. A careful inspection reveals that the dot is single-crystalline without evidence of pronounced dislocations or stacking faults (Fig. 1b and c). Extensive energy dispersive spectroscopy (EDS) and electron energy loss spectroscopy (EELS) studies revealed the presence of Mn (~5%) in the MnGe QDs (21); but importantly Mn aggregations were not detected within the resolution of the conventional TEM. No evident precipitates and phase separations of Mn_5Ge_3 and $Mn_{11}Ge_8$ were observed (21). It is noted that Mn doped single-crystalline $(In_{0.84}Mn_{0.16})As$ QDs were also found to maintain nearly perfect crystallinity although the Mn doping exceeded the solubility limit in InAs (22, 23).

Magnetic properties of the $Mn_{0.05}Ge_{0.95}$ quantum dots

Figure 2a and two corresponding insets show temperature-dependent hysteresis loops when the external magnetic field is parallel to the sample surface (in-plane). The field-dependent magnetization indicates a strong ferromagnetism above 400 K. The saturation magnetic moment per Mn atom is roughly estimated to be 1.8 μ_B at 5 K. A fraction of roughly 60% of Mn is estimated to be activated assuming that each Mn has a moment of 3 μ_B (9, 24–26). The Arrott plots (see the Methods) were also made to evaluate the Curie temperature (19, 27) as shown in Fig. 2b. We observe that even at 400 K the intercept $1/\chi$ (χ is susceptibility) on the H/M axis does not vanish, which means that χ still has a finite value and the Curie temperature has not been reached yet. By using the slope obtained at 400 K, a dashed line can be drawn as shown in Fig. 2b, in which a Curie temperature is projected to be beyond 400 K. This is in a good agreement with the data from the hysteresis loops showing the magnetic order above 400 K. Fig. 2c and corresponding inset show the temperature-dependent saturation and remnant moments per Mn ion, respectively. Both of them demonstrate weak temperature dependences and a substantial amount of magnetization moments remains even at 400 K. This phenomenon has also been observed recently in several nanostructure systems (22, 28–30). For example, 1% of Mn doping in Ge nanowires produces room temperature ferromagnetism and a weak temperature dependence of the saturation moments (29, 30); Cr doped InAs DMS QDs with the Cr/In flux ratio between 0.026 and 0.18 display a Curie temperature beyond 400 K while the remnant moment remains almost the same in the temperature range from 5 K to 300 K (28). With a Mn concentration of 16% in InAs QDs, the temperature-dependent magnetization keeps nearly constant until it reaches 400 K (but no electric-field dependence of magnetization was reported) (22). In contrast, the highest Curie temperature for III-V DMS bulk materials achieved so far only has a record of 185 K (31). While the discrepancy of Curie temperatures is still under investigation, the enhanced ferromagnetism in these nanostructures may be attributed to quantum confinement effect (22).

Zero field cooled (ZFC) and field cooled (FC) magnetizations were measured with a magnetic field of 100 Oe as shown in Fig. 2d. The magnetic moments do not drop to zero suggesting a high-Curie temperature beyond 400 K, which is in a good agreement with the Arrott plots in Fig. 2b. From these two curves, one can also infer the formation of a single phase in this material system (i.e. DMS QDs), which is surprisingly similar to the high-Curie temperature DMS $Mn_{0.05}Ge_{0.95}$ nanowires (32). The temperature-dependent coercivity is shown in Fig. 2d inset. Similar to the Mn_xGe_{1-x} nanowires (30), the

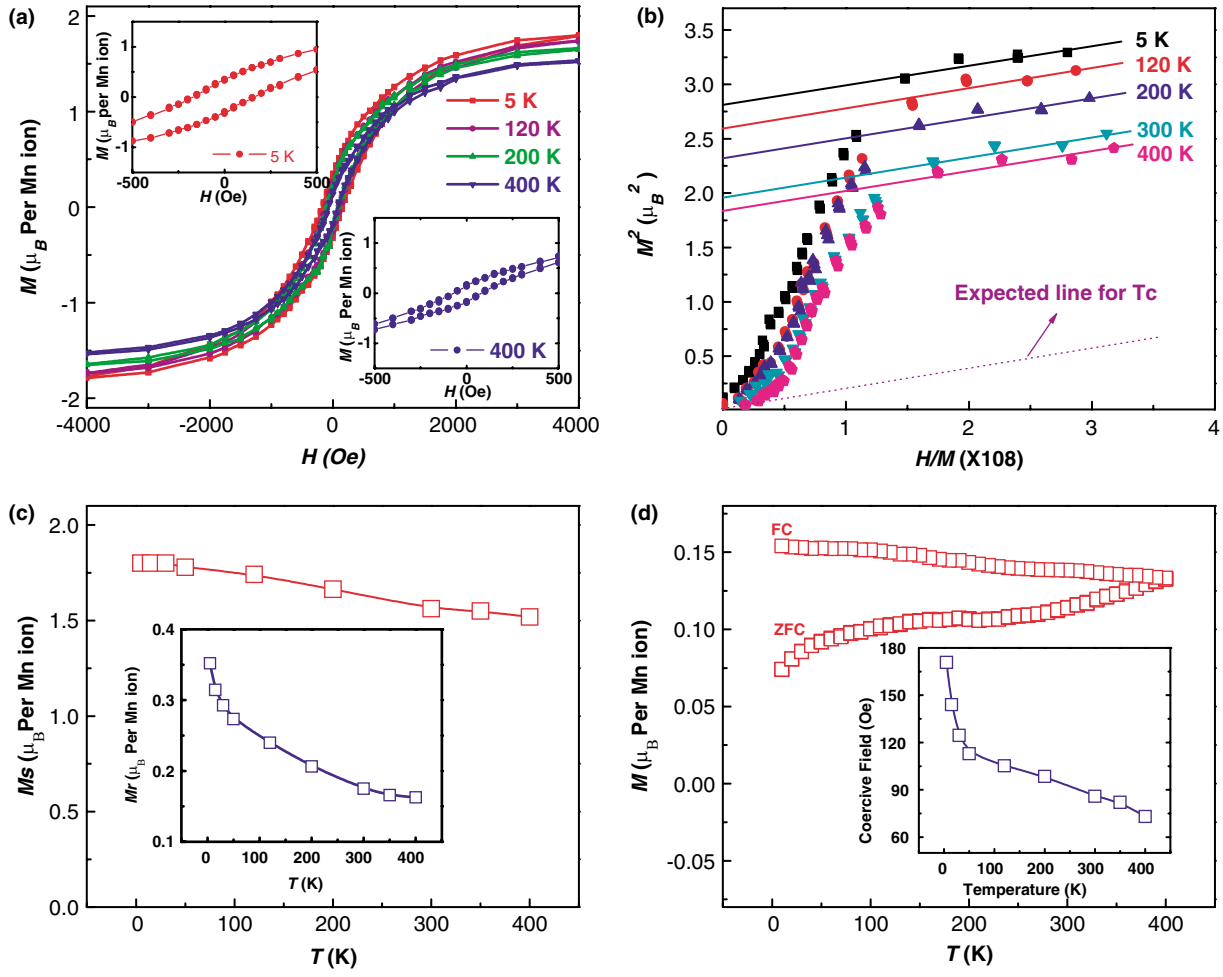

Fig. 2. Magnetic properties of the $Mn_{0.05}Ge_{0.95}$ quantum dots grown on a p-type Si substrate. (a) Hysteresis loops measured at different temperatures from 5 to 400 K. Insets are the hysteresis loops at 5 and 400 K. (b) The Arrott plots were made to obtain the Curie temperature. (c) The temperature dependence of saturation moments. The inset gives the remnant moments with respect to temperature. (d) Zero-field cooled and field cooled magnetizations of quantum dots with a magnetic field of 100 Oe, the inset shows the coercivity values at different temperatures. (Reproduced with permission from Ref. (21), copyright 2010 Nature Publishing Group.)

coercivity decreases from 170 Oe (at 5 K) to 73 Oe (at 400 K). The small coercivity in the entire temperature range measured features a soft ferromagnetism that originates from Mn ions diluted in the Ge matrix (33). The above magnetic properties support the fact that the $Mn_{0.05}Ge_{0.95}$ QDs exhibit a DMS type ferromagnetic order.

Atomic force microscopy (AFM) and magnetic force microscopy (MFM) measurements were carried out to investigate the morphology and ferromagnetism of the $Mn_{0.05}Ge_{0.95}$ QDs at 320 K, respectively. The dot density is about $6 \times 10^9\,cm^{-2}$ (Fig. 3a). The corresponding MFM image was taken by lifting up the MFM probe 25 nm above the topographic height of the sample in a phase detection mode (Fig. 3b). The appearance of bright-and-dark areas in the MFM image clearly shows the formation of magnetic domains in the $Mn_{0.05}Ge_{0.95}$ QDs, which is similar to (In, Mn)As DMS QDs (22). Fig. 3c–f shows enlarged MFM images of several individual $Mn_{0.05}Ge_{0.95}$ QDs. By reversing the tip magnetization, opposite contrast was observed for each dot indicating that the magnetic signals originated from the $Mn_{0.05}Ge_{0.95}$ QDs.

Metal-oxide-semiconductor capacitor devices

MOS capacitors were made by depositing 20 nm-thick MgO on top of the $Mn_{0.05}Ge_{0.95}$ QDs layer. The deposition of MgO layer is made by electron beam evaporation of a single crystal MgO source with a rate of ~1.0 Å/min measured by a quartz deposition monitor. Then the front and back sides were metalized with 200 nm-thick Au. Fig. 4a shows a cross-section TEM image of the MOS capacitor, consisting of electrodes (Au), MgO, $Mn_{0.05}Ge_{0.95}$ QDs, and *p*-type Si substrate.

Citation: Nano Reviews 2011, **2**: 5896 - DOI: 10.3402/nano.v2i0.5896

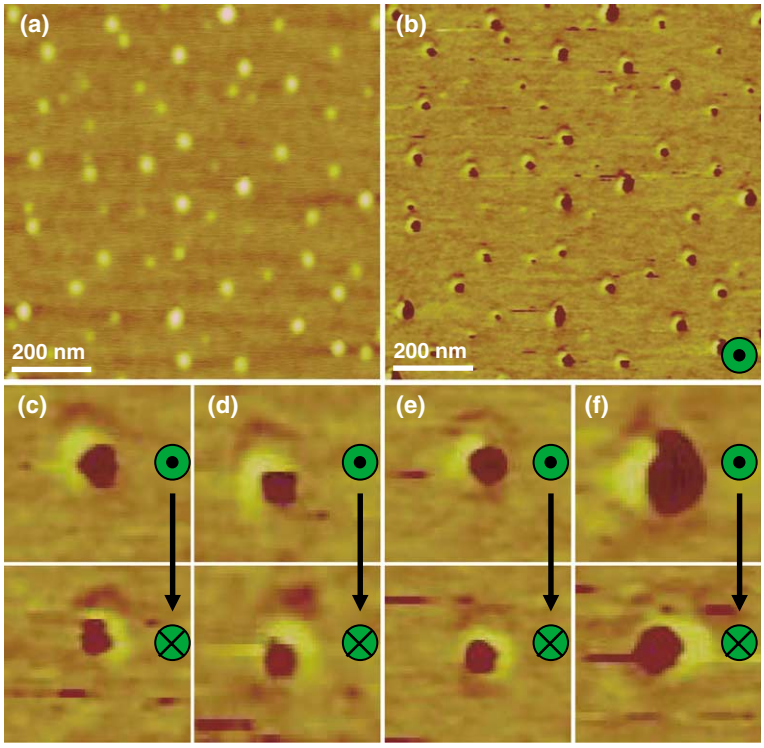

Fig. 3. AFM and MFM images of the Mn0.05Ge0.95 quantum dots measured at 320 K. (a) Typical AFM image of Mn0.05Ge0.95 quantum dots. (b) Corresponding MFM image with the tip magnetization pointing toward the sample. (c–f) Enlarged MFM images of individual quantum dots taken from (b). From these MFM measurements, opposite contrasts were observed when applying an opposite magnetization to the tip. (Reproduced with permission from Ref. (21), copyright 2010 Nature Publishing Group.)

Fig. 4b shows a schematic drawing of the MOS capacitor device structure. Capacitance-voltage curves were also measured at different temperatures (100 ~300 K, Fig. 5). Consistent with conventional MOS capacitors, the devices show transitions from hole accumulation to hole depletion when gate voltage changes from negative to positive biases. In the subsequent superconducting quantum interference device (SQUID) measurements, the top electrode was biased while the bottom one was grounded.

Electric-field controlled ferromagnetism

Figure 6 illustrates the electric-field controlled ferromagnetism performed at 100, 200, and 300 K, corresponding to 6a–c, 6d–f, and 6g–i, respectively (34). Due to the similarity of the data, we take the 100 K case as an example to describe the device operation (refer to Fig. 6a–c). Fig. 6a and b show the hysteresis loops by SQUID with negative and positive biases on the MOS gate at 100 K, respectively. Under a negative bias, the

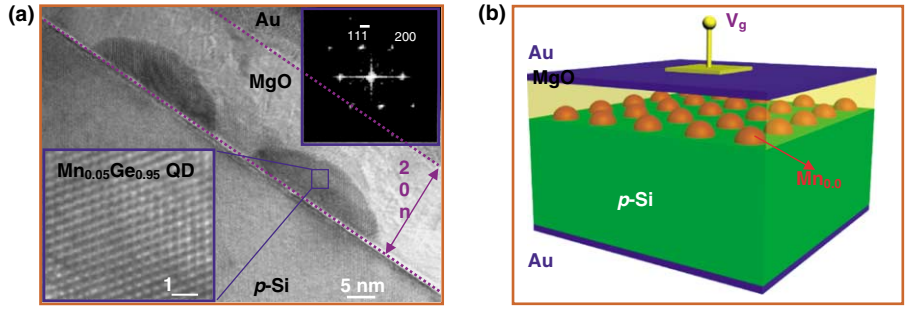

Fig. 4. Structure of MnGe MOS capacitor via TEM. (a) Cross-section HR-TEM images of the MnGe QDs grown on a *p*-Si substrate. (b) A schematic drawing of a MOS capacitor, consisting of electrodes (Au), MgO, MnGe QDs, and *p*-type Si substrate. Note that there is a thin MnGe wetting layer on top of Si (not shown in (b)). The wetting layer has a typical thickness of several Angstroms. (Reproduced with permission from Ref. (34), copyright 2010 American Chemical Society)

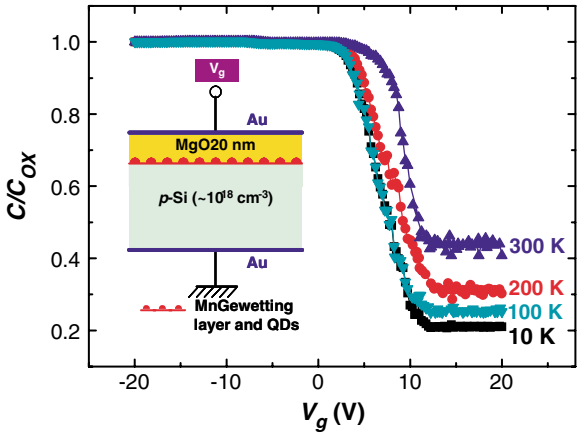

Fig. 5. Capacitance-voltage curves measured at 100, 200, and 300 K with a frequency of 1 MHz. It clearly shows a transition between the hole accumulation at negative bias and the hole depletion at positive bias. (Reproduced with permission from Ref. (34), copyright 2010 American Chemical Society.)

holes are attracted into the channel of the device (accumulation mode). In this circumstance, however, the hysteresis loop does not show a noticeable change (Fig. 6a). This can be explained by the fact that, even at zero volt, the QD device is already accumulated with enough holes to induce ferromagnetism; that is, the holes are sufficient to align the spins of a majority of the activated Mn ions in each individual dot. Further increasing negative bias does not change much on the hole concentration. On the contrary, with a positive bias, a large amount of holes are depleted into the *p*-type Si substrate so that hole-mediated effect is notably reduced. The saturation moment per Mn ion decreases about 2.5 times as the gate-bias increases from 0 to +40 V (Fig. 6b). Fig. 6c summarizes the change of remnant moments as a function of gate voltage. The inset in Fig. 6c displays an enlarged picture to clearly show the variation of the remnant moments with respect to the gate-bias. When the temperature was increased to 300 K (Fig. 6g–i), the saturation and the remnant moments were modulated by ~23% and ~50% (at +40 V), respectively, which clearly showed the room temperature controllable

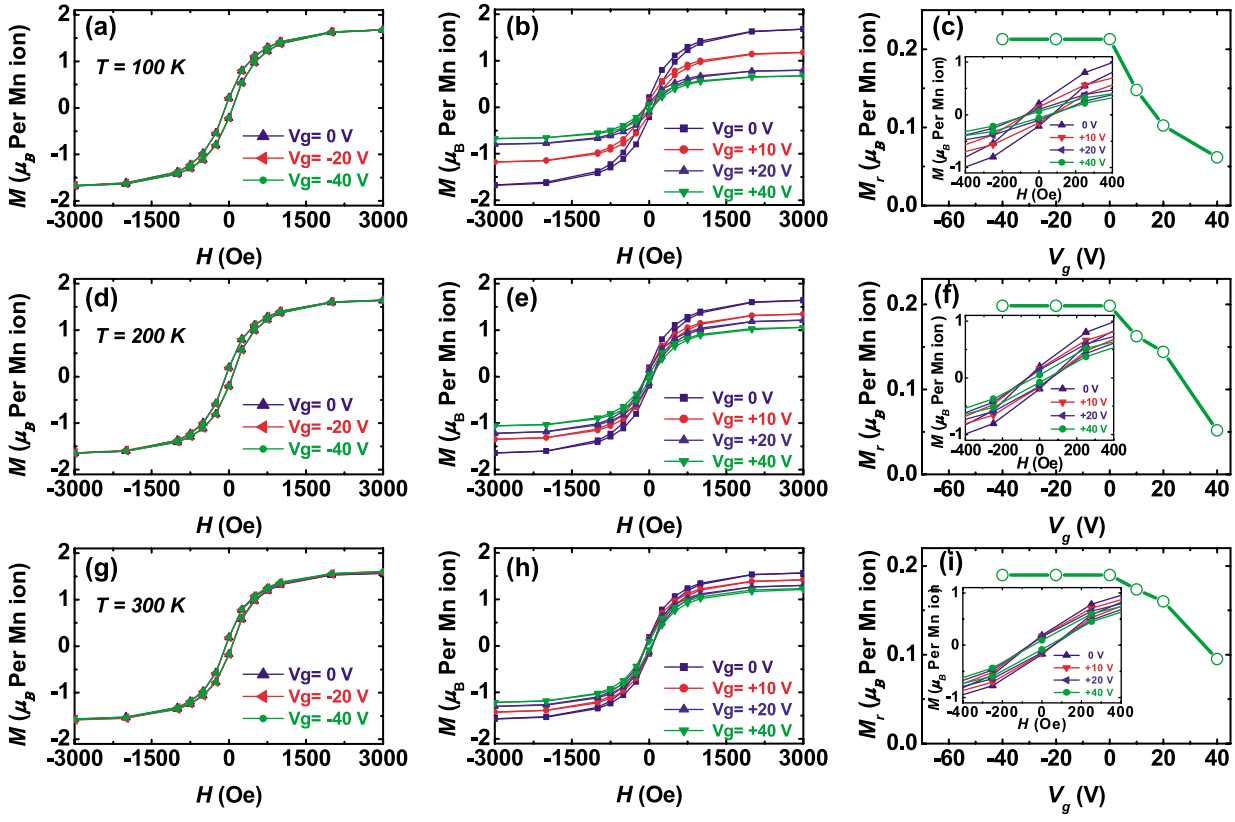

Fig. 6. Control of ferromagnetism of $Mn_{0.05}Ge_{0.95}$ quantum dots by applying electric field at 100 K (a–c), 200 K (d–f), and 300 K (g–i). (a, d, g) Hysteresis loops with zero and negative bias of −10, −20, and −40 V on the gate. (b, e, h) The hysteresis loops with zero and positive bias of +10, +20, and +40 V. (c, f, i) Remnant moments with respect to the gate-bias. Insets of (c, f, i) are enlarged figures from the central part of (b, e, h) to clearly show the change of remnant moments, respectively. (Reproduced with permission from Ref. (34), copyright 2010 American Chemical Society.)

Citation: Nano Reviews 2011, **2**: 5896 - DOI: 10.3402/nano.v2i0.5896

ferromagnetism, although it became less pronounced compared to those at 100 and 200 K (Fig. 6c and f).

Device simulations

Device simulations using the MEDICI package (35) were performed to understand the distributions of holes in a QD. The simulated device structure was designed to fit the experimental conditions. In the simulation, several physical models were adopted for accurate calculations including the freeze-out effect at low temperature, the Fermi-Dirac model for carrier occupations, and quantum mechanical corrections by invoking the Philip's band-gap widening effect (35). Fig. 7a–c shows the calculated hole concentrations as a function of the gate voltage at 100, 200, and 300 K, respectively. At zero bias, due to the quantum confinement between the $Mn_{0.05}Ge_{0.95}$ QDs and *p*-type Si (36), the hole concentration reaches 1.22×10^{18} and 2.08×10^{18} cm^{-3} for the top and center of the $Mn_{0.05}Ge_{0.95}$ QD, respectively (Fig. 7a, 100 K). By applying a negative bias, holes start to accumulate in the $Mn_{0.05}Ge_{0.95}$ QD, leading to an increased hole concentration. For instance, at –10 V, the hole concentration increases eight times (1.65×10^{19} cm^{-3}) in the center of the dot as calculated from Fig. 7a. However, by applying a positive voltage, the holes are depleted into the *p*-type Si substrate. The hole concentration changes dramatically on the top surface of the $Mn_{0.05}Ge_{0.95}$ QDs ($\sim 10^{10}$ cm^{-3}) while, at the center region, the concentration of $10^{14} \sim 10^{15}$ cm^{-3} remains in the voltage range of $+2 \sim +10$ V. Clearly, the top surface sensitively

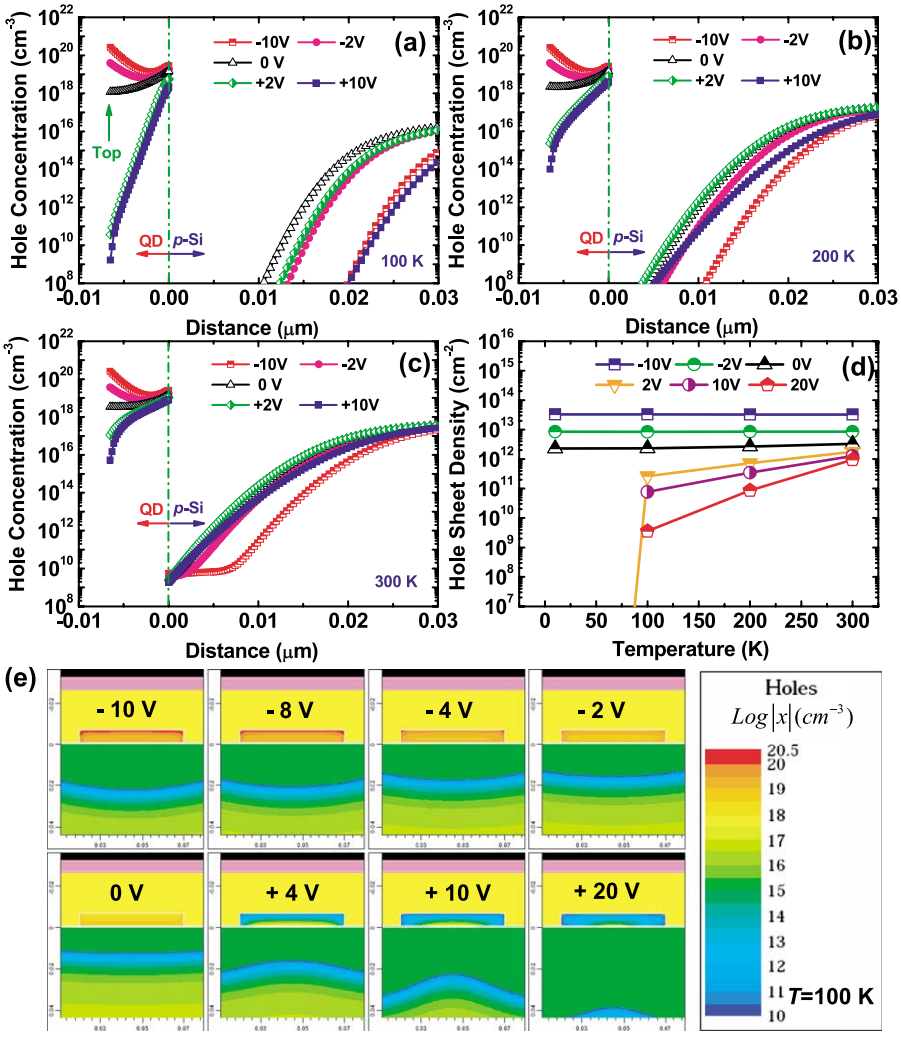

Fig. 7. Simulated hole distributions for a MOS device using the $Mn_{0.05}Ge_{0.95}$ quantum dots as the channel layer. (a, b, c) Simulated hole concentrations at 100, 200, and 300 K, respectively. Due to the Mn acceptor freeze-out effect, the depletion of holes inside the MnGe QDs is much more pronounced at 100 K compared with that of 300 K. (d) Integrated sheet densities of holes over the entire MnGe QD using a curvilinear integral method in Medici. Both temperature and voltage dependences of hole density are shown. (e) An example of hole redistribution map under different gate voltages at 100 K. (Reproduced with permission from Ref. (34), copyright 2010 American Chemical Society.)

responds to the gate-bias. Fig. 3e illustrates the redistribution of holes in QD with gate-biases at 100 K. It is noted that the hole concentration in the $Mn_{0.05}Ge_{0.95}$ QD decreases as the bias increases from -10 to $+20$ V; this result further confirms the hole accumulation, depletion, and inversion processes. Similarly, we have performed the simulations at 200 and 300 K in Fig. 7b and c, respectively. At $+10$ V, the top of the QD exhibits a high concentration of 10^{16} cm^{-3} at 300 K in comparison with that of 100 K ($\sim 10^{10}$ cm^{-3}), possibly resulted from the more activation of the Mn impurities and, thus, a higher doping level of Mn in the QD. Based on these simulation results, we can conclude that the depletion process at high temperatures is not as strong as those at low temperatures. This explains the reduced controllability of ferromagnetism when the temperature approaches 300 K. Since the hole concentration varies with position inside the $Mn_{0.05}Ge_{0.95}$ QD, it is necessary to integrate the entire area of the QD and obtain a sheet density as an 'effective' hole density as shown in Fig. 7d. In the accumulation mode (under zero and negative gate-biases), the hole concentration does not have a noticeable temperature dependence from 10 to 300 K. However, in the depletion mode (positive biases), the holes were significantly depleted out of the $Mn_{0.05}Ge_{0.95}$ QD when the temperature decreases to below 100 K, primarily due to the freeze-out effect of the Mn acceptors (37).

Physical model

Energy band diagrams of MgO/$Mn_{0.05}Ge_{0.95}$ QD/Si and MgO/$Mn_{0.05}Ge_{0.95}$ wetting layer/Si are schematically shown in Fig. 8a and c, respectively. By solving the Schrodinger Equation for a rectangular quantum well with finite barriers (38), we estimated that the $Mn_{0.05}Ge_{0.95}$ QDs have five quantized energy levels with $E_1 = 21$ meV, $E_2 = 81$ meV, $E_3 = 167$ meV, $E_4 = 258$ meV, and $E_5 = 331$ meV as shown in Fig. 8a. Among these levels, E_1 represents the ground state (i.e. the lowest energy level). In contrast, the wetting layer exhibits a higher ground state of E_1^* with a value of 142 meV. Since the energy of the ground state is much lower in the QDs, the majority of the holes would prefer to transfer into the dots, giving rising to a higher density of holes compared with that of the wetting layer. Fig. 8b shows a schematic drawing of the QDs and the wetting layer in the real space. The energy band diagrams are also provided at the bottom of Fig. 8b to visualize the transport of the holes. Note that due to the relatively large diameter of the $Mn_{0.05}Ge_{0.95}$ QDs (>30 nm), the quantum confinement in the horizontal direction is not significant compared with that in the vertical direction (perpendicular to the Si

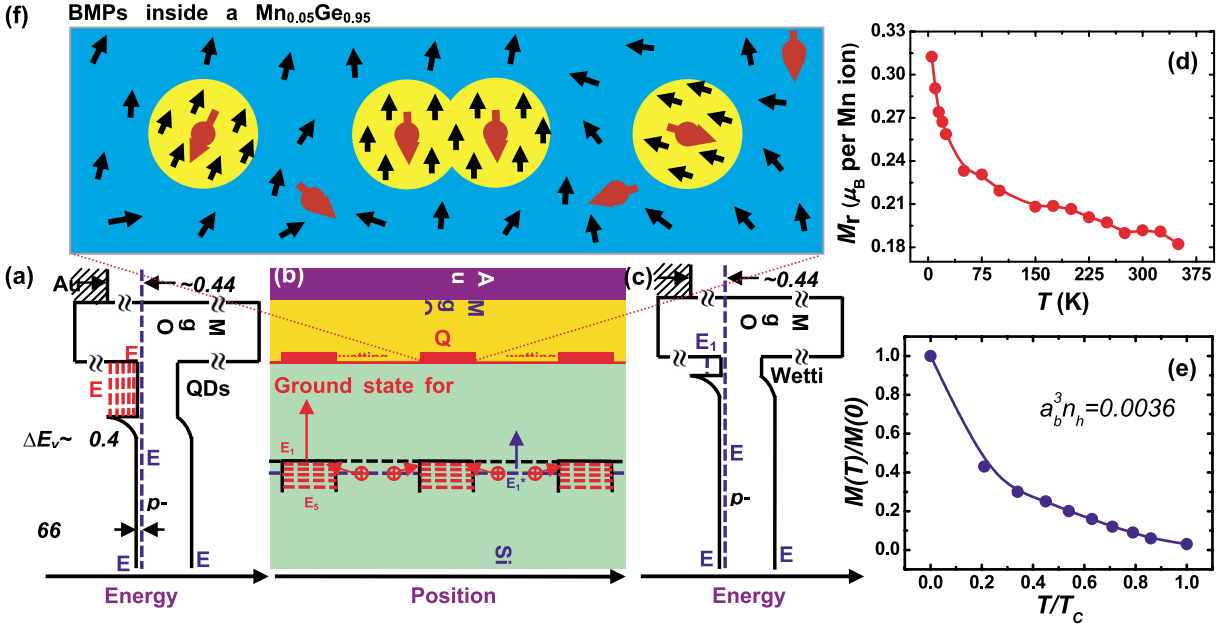

Fig. 8. Energy band diagrams and a magnetic polaron model in the MnGe QDs. (a, c) The energy band diagrams of MgO/MnGe QD/Si and MgO/MnGe wetting layer/Si, respectively. (b) A schematic drawing of the QDs and the wetting layer in real space. The energy band diagrams are also provided in the bottom to visualize the quantum confinement of the holes in the dots. (d) Remnant moments as a function of temperature at zero bias. A concave upward curve is observed. (e) Normalized remnant moments as a function of T/T_c. The concave nature is similar to that in (d). (f) Formation of BMPs inside a single MnGe QD. Small and large arrows show Mn impurity and hole spins, respectively. Some of BMPs are shown to overlap with each other to enhance ferromagnetism when a high density is developed (top panel). (Reproduced with permission from Ref. (34), copyright 2010 American Chemical Society.)

Citation: Nano Reviews 2011, **2**: 5896 - DOI: 10.3402/nano.v2i0.5896

surface, or along the height of the QDs). To explore the origin of the ferromagnetism in this material system, we plot the measured remnant magnetizations as a function of temperature, $M(T)$ (Fig. 8d), at zero bias, as the nature of $M(T)$ has been found crucial in understanding the underlying mechanism of DMS ferromagnetism (39). The concave upward shape of $M(T)$ shown in Fig. 8d is consistent with earlier reports of MnGe DMS (9, 40), which agrees well qualitatively with the percolation type of ferromagnetic transition. We also compare the dependence of calculated $M(T)$ (Fig. 8e) using the percolation theory approach based on magnetic polaron model proposed by Kaminski and Das Sarma (41),

$$M(T)/M(0) = \beta[0.86 + (a_b^3 n_n)^{1/3} \ln(T_c/T)], \quad (1)$$

where $M(0)$ is the remnant moment at zero temperature; β is the 'infinite' cluster volume of overlapping spheres; a_b is the calculated Bohr radius (42). It must be emphasized that given the minimal nature of the model, one can only hope for a qualitative agreement and it is incorrect to try getting a quantitative agreement between theory and experiment by tuning the parameters of the above model (39).

On the basis of the above agreement on the shape of $M(T)$, we can construct a physical model based on the concept of bound magnetic polarons (BMPs) to explain the observed field controlled ferromagnetism (43). BMPs are regions of large magnetization resulting from all parallel polarized Mn spins. They are formed as a consequence of exchange interactions between the spins of localized carriers and magnetic ions, as illustrated in Fig. 8f. Since the Mn doping concentration in our system is much larger than the hole concentration due in part to the compensation by Mn interstitials, BMPs could be developed with localized holes and a large number of Mn impurities around the hole localization center (41). One can approximate several Mn ions to a sphere within a radius of r_h, and assume that the Mn impurities contained inside this sphere interact with the hole and align their spins antiparallel to the hole spin that results in the formation of a BMP (44). The radius, r_h, grows with decreasing temperature given by $r_h \sim (a_b/2)\ln(J_0/k_BT)$ (45), where J_0 characterizes the strength of the exchange between carriers and magnetic ion. It was also shown that the nearby BMPs align ferromagnetically *via* effective coupling mediated by Mn spins lying in between the BMPs (45, 46). As a result, BMPs start to overlap and form percolated clusters aligned ferromagnetically as temperature decreases (Fig. 8f) (41, 44, 46–49). From both theoretical calculations and experimental data, the MP formation was also found to be more favorable when the system dimension was reduced, particularly in the QDs case (49–51). This phenomenon was explained by the fact that the quantum confinement could localize carriers in the proximity of magnetic ions and further strengthen the exchange interactions (49–51). More interestingly, the binding energy of the MPs was remarkably enhanced when the system dimension shrinks, resulting in a higher T_c in contrast to those of bulk materials (49, 52).

The above physical picture can be applied to explain the electric-field control of ferromagnetism in the $Mn_{0.05}Ge_{0.95}$ DMS system. The gate-controlled hole carriers in the $Mn_{0.05}Ge_{0.95}$ QDs may influence the formation of MPs and their interactions. If the holes density is sufficient, they can effectively mediate interactions between nearly all MPs in a dot (53). When the hole density decreases in the depletion process, however, the amount of MPs can be reduced; and meanwhile, the overlapped MPs may start to uncouple and even disappear at low carrier densities, as illustrated in the outer MPs in Fig. 8f, thus reducing the net magnetization moments. When the temperature increases toward room temperature, the MPs are subject to thermal fluctuation and become less stable compared to those at lower temperatures (49, 54). This is in agreement with the fact that, the saturation moment decreases with increasing the temperature (zero bias). As mentioned earlier, the hole depletion process became less pronounced at 300 K when compared with that of low temperatures, for example, with +10 V, the holes on top of the QD do not change as much as those at 100 and 200 K (Fig. 7a–c). This indicates that the QDs contain a large density of holes and possibly a high density of MPs at high temperatures because of more activation of the Mn acceptors, leading to a weak dependence of magnetization on the bias field. This analysis qualitatively explains the weak controllability of ferromagnetism at elevated temperatures.

Summary and prospective

Interest in DMS ferromagnetism is motivated by the possibility to engineer systems that combine many of the technologically useful features of ferromagnetic and semiconducting materials. This goal has been achieved to an impressive degree in (III, Mn)-V DMSs and further progress can be anticipated in the future. However, due to the low T_c of (III, Mn)-V DMSs, the spintronics research seemingly reaches a critical bottleneck, where achieving a high T_c DMS becomes an intriguing and challenging task. Fortunately, the MnGe material system offers a possible route toward higher T_c. A high T_c in excess of 400 K can be obtained and is presumably attributed to the quantum confinement effect, which strengthens the hybridization between the localized Mn impurities and iterant holes. Bound magnetic polarons may also exist since this system falls into a regime where Mn concentrations are much larger than that of holes.

It is well known that in order to achieve functioning spintronic devices working at ambient temperatures, it requires the following criteria: (i) the ferromagnetic

transition temperature should safely exceed room temperature, (ii) the mobile charge carriers should respond strongly to changes in the ordered magnetic state, and (iii) the material should retain fundamental semiconductor characteristics, including sensitivity to doping and light, and electric-fields produced by gate charges. For more than a decade, these three key issues have been the focus of intense experimental and theoretical research. Progress has been also made in achieving field controlled ferromagnetism in (III, Mn)As system, even though the controllability remains at low temperatures because of low T_c. Therefore, the critical challenge now is either to continue increasing T_c in (III, Mn)As or to look for a new DMS system with both high-Curie temperature ($T_c >>$ 300 K) and the field controlled ferromagnetism to satisfy all these three criteria. The experimental results of field controlled ferromagnetism in the MnGe QDs suggest that the ferromagnetism in this system sensitively responds to the electrical field via the hole-mediated effect, similar to that in (III, Mn)As system. Therefore, with a much higher T_c compared with III-V DMS, the MnGe quantum dots could become one of the most promising candidates to achieve room temperature operation.

Acknowledgements

We gratefully acknowledge the financial support from the Western Institute of Nanoelectronics (WIN), the Intel Spin-Gain FET project, and the Australian Research Council. YW thanks the Queensland International Fellowship.

Conflict of interest and funding

There is no conflict of interest in the present study for any of the authors.

References

1. Awschalom DD, Loss D, Samarth N. Semiconductor spintronics and quantum computation. Berlin: Springer-Verlag; 2002: 1–12.
2. Chiba D, Matsukura F, Ohno H. Electrical magnetization reversal in ferromagnetic III-V semiconductors. J Appl Phys D: Appl Phys 2006; 39: R215–25.
3. Datta S, Das B. Electronic analog of the electro-optic modulator. Appl Phys Lett 1990; 56: 665–7.
4. Philip J, Punnoose A, Kim BI, Reddy KM, Layne S, Holmes JO, et al. Carrier-controlled ferromagnetism in transparent oxide semiconductors. Nat Mater 2006; 5: 298–304.
5. Kanki T, Tanaka H, Kawai T. Electric control of room temperature ferromagnetism in a $Pb(Zr_{0.2}ti_{0.8})O_3/La_{0.85}ba_{0.15}MnO_3$ field-effect transistor. Appl Phys Lett 2006; 89: 242506.
6. Dietl T, Ohno H. Engineering magnetism in semiconductors. Mater Today 2006; 9: 18–26.
7. Nepal N, Luen MO, Zavada JM, Bedair SM, Frajtag P, El-Masry NA. Electric-field control of room temperature ferromagnetism in Iii-N dilute magnetic semiconductor films. Appl Phys Lett 2009; 94: 132505.
8. Dietl T, Ohno H, Matsukura F, Cibert J, Ferrand D. Zener model, description of ferromagnetism in zinc-blende magnetic semiconductors. Science 2000; 287: 1019–22.
9. Park YD, Hanbicki AT, Erwin SC, Hellberg CS, Sullivan JM, Mattson JE, et al. A Group-IV ferromagnetic semiconductor: Mn_xGe_{1-X}. Science 2002; 295: 651–4.
10. Chen J, Wang KL, Galatsis K. Electrical field control magnetic phase transition in nanostructured Mn_xGe_{1-X}. Appl Phys Lett 2007; 90: 012501.
11. Ohno H, Chiba D, Matsukura F, Omiya T, Abe E, Dietl T, et al. Electric-field control of ferromagnetism. Nature 2000; 408: 944–6.
12. Chiba D, Matsukura F, Ohno H. Electric-field control of ferromagnetism in (Ga,Mn)As. Appl Phys Lett 2006; 89: 162505.
13. Chiba D, Sawicki M, Nishitani Y, Nakatani Y, Matsukura F, Ohno H. Magnetization vector manipulation by electric-fields. Nature 2008; 455: 515–8.
14. Weisheit M, Fahler S, Marty A, Souche Y, Poinsignon C, Givord D. Electric-field-induced modification of magnetism in thin-film ferromagnets. Science 2007; 315: 349–51.
15. Jungwirth T, Sinova J, Masek J, Kucera J, MacDonald AH. Theory of ferromagnetic (III,Mn)V semiconductors. Rev Mod Phys 2006; 78: 809–64.
16. Bolduc M, Awo-Affouda C, Stollenwerk A, Huang MB, Ramos FG, Agnello G, et al. Above room temperature ferromagnetism in Mn-Ion implanted Si. Phys Rev B 2005; 71: 033302.
17. Pinto N, Morresi L, Ficcadenti M, Murri R, D'Orazio F, Lucari F, et al. Magnetic and electronic transport percolation in epitaxial $Ge_{1-X}Mn_x$ films. Phys Rev B 2005; 72: 165203.
18. Wang Y, Zou J, Zhao Z, Han X, Zhou X, Wang KL. Direct structural evidences of $Mn_{11}Ge_8$ and Mn_5Ge_2 clusters in $Ge_{0.96}Mn_{0.04}$ thin films. Appl Phys Lett 2008; 92: 101913.
19. Li AP, Wendelken JF, Shen J, Feldman LC, Thompson JR, Weitering HH. Magnetism in Mn_xge_{1-X} semiconductors mediated by impurity band carriers. Phys Rev B 2005; 72: 195205.
20. Knobel R, Samarth N, Crooker SA, Awschalom DD. Spin-polarized quantum transport and magnetic field-dependent carrier density in magnetic two-dimensional electron gases. Physica E: Low-Dimen Sys Nanostr 2000; 6: 786–9.
21. Xiu F, Wang Y, Kim J, Hong A, Tang J, Jacob AP, et al. Electric-field-controlled ferromagnetism in high-curie-temperature $Mn_{0.05}ge_{0.95}$ quantum dots. Nat Mater 2010; 9: 337–44.
22. Jeon HC, Jeong YS, Kang TW, Kim TW, Chung KJ, Jhe W, et al. $(In_{1-X}Mn_x)As$ diluted magnetic semiconductor quantum dots with above room temperature ferromagnetic transition. Adv Mater 2002; 14: 1725–8.
23. Chen YF, Lee WN, Huang JH, Chin TS, Huang RT, Chen FR, et al. Growth and magnetic properties of self-assembled (In, Mn)As quantum dots. J Vacuum Sci Tech B: Microelectr Nano Struct 2005; 23: 1376–8.
24. Stroppa A, Picozzi S, Continenza A, Freeman AJ. Electronic structure and ferromagnetism of Mn-Doped group-IV semiconductors. Phys Rev B 2003; 68: 155203.
25. Schulthess TC, Butler WH. Electronic structure and magnetic interactions in Mn doped semiconductors. J Appl Phys 2001; 89: 7021–3.
26. Schilfgaarde MV, Mryasov ON. Anomalous exchange interactions in III-V dilute magnetic semiconductors. Phys Rev B 2001; 63: 233205.
27. Ohno H. Making nonmagnetic semiconductors ferromagnetic. Science 1998; 281: 951–6.
28. Zheng YH, Zhao JH, Bi JF, Wang WZ, Ji Y, Wu XG, et al. Cr-doped InAs self-organized diluted magnetic quantum dots

Citation: Nano Reviews 2011, 2: 5896 - DOI: 10.3402/nano.v2i0.5896

with room-temperature ferromagnetism. Chin Phys Lett 2007; 24: 2118–21.
29. Kulkarni JS, Kazakova O, Erts D, Morris MA, Shaw MT, Holmes JD. Structural and magnetic characterization of $Ge_{0.99}Mn_{0.01}$ nanowire arrays. Chem Mat 2005; 17: 3615–9.
30. van der Meulen MI, Petkov N, Morris MA, Kazakova O, Han X, Wang KL, et al. Single crystalline $Ge_{1-X}Mn_x$ nanowires as building blocks for nanoelectronics. Nano Lett 2008; 9: 50–6.
31. Wang M, Campion RP, Rushforth AW, Edmonds KW, Foxon CT, Gallagher BL. Achieving high Curie temperature in (Ga,Mn)As. Appl Phys Lett 2008; 93: 132103.
32. Cho YJ, Kim CH, Kim HS, Lee WS, Park S-H, Park J, et al. Ferromagnetic $Ge_{1-X}m_x$ (M = Mn, Fe, and Co) Nanowires. Chem Mat 2008; 20: 4694–702.
33. Kazakova O, Kulkarni JS, Holmes JD, Demokritov SO. Room-temperature ferromagnetism in $Ge_{1-X}mn_x$ nanowires. Phys Rev B 2005; 72: 094415.
34. Xiu F, Wang Y, Kim J, Upadhyaya P, Zhou Y, Kou X, et al. Room-temperature electric-field controlled ferromagnetism in $Mn_{0.05}Ge_{0.95}$ quantum dots. ACS Nano 2010; 4: 4948–54.
35. MEDICI. Two-dimensional semiconductor device simulation program. Palo Alto, CA: Technology Modeling Associates, 2005.
36. Wang KL, Thomas SG, Tann MO. SiGe band engineering for MOS, CMOS and quantum effect devices. J Mater Sci-Mater Electron 1995; 6: 311–24.
37. Sze S. Physics of semiconductor devices, second ed. New York: Wiley; 1981.
38. Schiff LI. Quantum mechanics, third ed. New York: McGraw-Hill; 1993.
39. Das Sarma S, Hwang EH, Kaminski A. Temperature-dependent magnetization in diluted magnetic semiconductors. Phys Rev B 2003; 67: 155201.
40. Li AP, Shen J, Thompson JR, Weitering HH. Ferromagnetic percolation in Mn_xge_{1-X} dilute magnetic semiconductor. Appl Phys Lett 2005; 86: 152507.
41. Kaminski A, Das Sarma S. Polaron percolation in diluted magnetic semiconductors. Phys Rev Lett 2002; 88: 247202.
42. Berciu M, Bhatt RN. Effects of disorder on ferromagnetism in diluted magnetic semiconductors. Phys Rev Lett 2001; 87: 107203.
43. Furdyna JK, Kossut J, editors. Diluted magnetic semiconductors and semimetals. Vol. 25. London: Academic Press; 1988.
44. Sangaletti L, Canova FF, Drera G, Salvinelli G, Mozzati MC, Galinetto P, et al. Magnetic polaron percolation on a rutile lattice: A geometrical exploration in the limit of low density of magnetic impurities. Phys Rev B 2009; 80: 033201.
45. Bhatt RN, Berciu M, Kennett MP, Wan X. Diluted magnetic semiconductors in the low carrier density regime. J Supercond 2002; 15: 71–83.
46. Wolff PA, Bhatt RN, Durst AC. Polaron-polaron interactions in diluted magnetic semiconductors. J Appl Phys 1996; 79: 5196–8.
47. Coey JMD, Venkatesan M, Fitzgerald CB. Donor impurity band exchange in dilute ferromagnetic oxides. Nat Mater 2005; 4: 173–9.
48. Durst AC, Bhatt RN, Wolff PA. Bound magnetic polaron interactions in insulating doped diluted magnetic semiconductors. Phys Rev B 2002; 65: 235205.
49. Bhattacharjee AK, la Guillaume CBA. Exciton magnetic polaron in semimagnetic semiconductor nanocrystals. Phys Rev B 1997; 55: 10613–20.
50. Yakovlev DR, Uraltsev IN, Ossau W, Landwehr G, Bicknell-Tassius RN, Waag A, et al. Two-dimensional exciton magnetic polaron in semimagnetic quantum wells. Surf Sci 1992; 263: 485–90.
51. Maksimov AA, Bacher G, McDonald A, Kulakovskii VD, Forchel A, Becker CR, et al. Magnetic polarons in a single diluted magnetic semiconductor quantum dot. Phys Rev B 2000; 62: R7767–70.
52. Mackowski S, Gurung T, Nguyen TA, Jackson HE, Smith LM, Kossut J, et al. Optically controlled magnetization of zero-dimensional magnetic polarons in cdmnte self-assembled quantum dots. Phys Status Solidi C 2004: 656–59.
53. MacDonald AH, Schiffer P, Samarth N. Ferromagnetic semiconductors: Moving beyond (Ga,Mn)As. Nat Mater 2005; 4: 195–202.
54. Stirner T, Hagston WE, Harrison P, Goodwin JP. Exciton magnetic polarons in quantum wells. J Appl Phys 1994; 75: 3466–71.

***Faxian Xiu**
Electrical Engineering Department
63-109 Engineering IV Building
Los Angeles, CA, 90095-1594, USA
Email: xiu@ee.ucla.edu

***Kang L. Wang**
Electrical Engineering Department
66-147C Engineering IV Building
Los Angeles, CA, 90095-1594, USA
Email: wang@ee.ucla.edu